

PILASTRI DI MURATURA SOGGETTI A FORZE ORIZZONTALI:
UN CONFRONTO TRA MODELLAZIONE AGLI ELEMENTI FINITI E
RISULTATI SPERIMENTALI

MASONRY COLUMNS UNDER HORIZONTAL LOADS: A
COMPARISON BETWEEN FINITE ELEMENT MODELLING AND EXPERIMENTAL
RESULTS

U. Andreaus, G. Ceradini, M. Cerone, P. D'Asdia

Istituto di Scienza delle Costruzioni, Facoltà di Ingegneria,
Università di Roma "La Sapienza", Via Eudossiana 18, 00184 ROMA

SOMMARIO

La nota presenta i risultati sperimentali, ottenuti su una coppia di pilastri di muratura soggetti a carichi verticali ed orizzontali, mostrando l'importanza dell'"effetto arco" nel determinare il carico ultimo e il comportamento sotto azioni cicliche di tali strutture.

I risultati delle prove sono anche stati usati per verificare i risultati ottenuti per mezzo di un modello matematico per l'analisi delle murature basato su precedenti studi degli Autori su elementi strutturali dotati di legami costitutivi multilineari governati da parametri di danno.

SUMMARY

The paper presents the experimental results, obtained on a couple of masonry columns under vertical and horizontal loads, showing the importance of the arching effect in determining the ultimate load and the behaviour under cyclic actions of such structures.

The test results are also used to verify the results obtained by a mathematical model for the analysis of masonry based on previous studies of the Authors about structural elements exhibiting multilinear constitutive laws ruled by damage parameters.

1. GENERALITIES

The effect of arching as load carrying capacity of masonry piers and walls subjected to monotonically increasing lateral forces, as long as the tensile strength has been attained, is evaluated from an experimental point of view; the results of experimental tests carried out by two tuff brick masonry piers are compared with those ones obtained by calculations carried out by both an approximated theoretical method, based on limit analysis (1) and very simple to be used, and a non linear analysis, performed by discretizing the structure into finite elements comprised of sub-assemblages of mono-dimensional members.

The onset of the arching effect and its importance in determining the load carrying capacity of piers has been well shown experimentally, by both the crack distribution and the value of the ultimate lateral force, which is much greater than one corresponding to a bending and shearing behaviour.

The good agreement reached between numerical and experimental results has shown the reliability of the adopted schematizations, because the exhibited differences are most due to the approximations introduced in the failure domains of material and in the force-displacement diagrams, and to the degree of discretization adopted in the numerical simulation.

At the present time the authors have performed the analysis of the same piers under cyclic lateral forces; the material behaviour under cyclic loading has been obtained by results of experimental tests carried out by analogous piers, axially loaded by attaining the ultimate strength at each cycle.

2. EXPERIMENTAL TESTS

Two tuff brick masonry piers have been investigated having dimensions 33x33x75 cm, shown in Fig. 1. The piers are supported at the edges by means of two very stiff steel beams inserted between the plates of a press, which gives to each one of them an initial vertical load $N = 2.5 \text{ t}$ ($\sigma = 2.3 \text{ Kg/cm}^2$), and at the bottom and the top by means of two horizontal frames; a lateral force F , monotonically increasing, is applied by an hydraulic jack connected in series to a dynamometer and, in order to account for vertical supports' imperfections, one acts on the press at each loading increment of the jack, so that relative displacement between the pier edges are dropped out.

The test instrumentation, shown in Fig. 1, is capable of measuring strains ϵ at selected points of the central and external sections of the piers (inductance transducers have been located at both the faces of each pier, parallel to the load plane), relative vertical displacements, between the bottom and the top of each pier (centesimal collimators have been placed between the steel beams), and eventually horizontal displacements of the central sections (centesimal collimators). Axial force N 's changes are measured by the control apparatus of the press at each loading increment of the force F .

The crack distribution at the end of the test has been depicted in Fig. 2. The crack distribution, even if different behaviours have been exhibited by the two piers, shows the effect of arching; the pressure curve has been clearly identified in pier 2, whereas slippage of horizontal joints, occurred before the collapse, makes it less easily understandable.

The experimental results are shown, as far as the distribution of the most significant quantities, in the Figs. 3 and 4, where they are compared with the results obtained by numerical analysis carried out on the basis of the schematizations of sect. 3.

The onset of the effect of arching is shown by the increment of the axial force N as the lateral force F increases.

The relation between N and F is nearly linear; the vertical branch in the experimental diagram corresponds to an initial bending-compression behaviour due to pre-loading.

The behaviour linearity is corroborated by $F-\delta$ and $F-\epsilon$ diagrams shown in the Figs. 4 and 5 respectively; namely, the linear distribution of the ϵ_{\max} as F va-

ries (Fig. 5) allows to assume the distribution of normal stresses to be proportional to strains and hence permits to argue the diagrams σ shown in fig. 6.

3. FINITE ELEMENT MODELLING AND COMPARISON WITH EXPERIMENTAL RESULTS

The experimental tests described in the previous section have been numerically simulated, by discretizing the pier into finite elements, as shown in Fig. 7. The finite element technique is based on subassemblages of mono-dimensional members as described more in detail in (2); the individual finite element is comprised of six truss members located on the sides and diagonals of a square.

3.1 Parameter identification

The mechanical and geometrical parameters of the single finite elements have been identified on the basis of experimental results presented in sect. 2, as far as both the constitutive law of the single truss member and the failure domains of the entire finite element are concerned.

The force-displacement experimental diagram is shown in Fig. 9, while the tri-linear constitutive law adopted for the single truss members is presented in Fig. 10. Thus masonry has been assumed to be isotropic with failure domain $\sigma_v - \sigma_o$ shown in Fig. 8, where it is compared with experimental results; the solid and dashed lines represent respectively the domains generated by using the tri-linear schematization of constitutive law of Fig. 10 and the elastic-perfectly plastic constitutive law. As shown in the following paragraphs, the two constitutive laws lead to the same good agreement with experimental results, provided that the brittle limit strength in tension of the tri-linear law is suitably larger than the corresponding ductile limit strength of the elastic-plastic law.

3.2 Monotonically increasing loads

The numerical results seem to satisfactorily fit the corresponding experimental data, as shown by the comparison presented in Figs. 3 and 4.

As far as the elastic-plastic model is concerned the differences between experimental and theoretical diagrams of Figs. 3 and 4 are due to both the adopted discretization by only four elements on the cross section (the element dimensions are hence comparable with those one of the compressed section portion), and primarily the approximation of the assumed constitutive law; in fact, the model, allowing for unreal ductility of material, gives, even in the collapse proximity, load-carrying capacity in tension to the diagonals and hence underestimates the value of the compression N in the cross-section.

Adopting the tri-linear schematization of the constitutive law allows to achieve an even better agreement between theoretical behaviour and experimental data; in fact figure 3 shows that experimental and theoretical lateral load-axial force diagrams have practically the same slope. Figure 4 shows that both elastic-plastic model and tri-linear schematization give an ultimate load practically equal to the experimental one, while the tri-linear schematization allows a better approximation of the force-displacement path up to the ultimate load. Moreover, numerical investigation has been extended to a displacement range wider than the experimental one.

The same considerations can be expressed about the differences among the theoretical and experimental σ diagrams in the cross-section (Fig. 6); the linear distribution of normal stress σ , which has been experimentally noticed, is confirmed by

the calculations, as reported also in (3).

Eventually the deformed shape given by numerical analysis and the corresponding crack distribution, shown in Fig. 11 exhibit a good agreement with experimental results.

3.3 Cyclic loading

The same pier has been modelled on the basis of the tri-linear schematization and analysed under cyclic lateral displacements simulating an experimental test where two hydraulic jacks alternatively push each side of the specimen. Figure 12 shows the lateral force-displacement diagram, where the ultimate strength is attained at the end of each loading cycle; the loading history is depicted in the same figure. It is worth to be noticed that in this loading history slippage due to crack opening is exhibited only after the second reversal point and that the percentual reductions of the ultimate strength during the loading path are: 100, 70, 60.

Figure 13 shows the first cycle of a further loading program where slippage due to crack opening attains significant values.

4. SIMPLIFIED METHOD VIA LIMIT ANALYSIS

A numerical comparison has been carried out also by using simplified relationships formulated by limit analysis; on the basis of this simplified procedure, described more in detail in (1), the ultimate value of the lateral force is given by:

$$F_u = 1.5 \frac{\sigma_u l s^3}{l^2 - a^2} \text{ or } F_u = 0.75 \tau_u s^2 \quad (1)$$

where σ_u and τ_u are the ultimate normal and shear stresses respectively, "a" is the load-point; the normal and shear stress distributions at the central and external cross-section are assumed to be linear (according to both experimental and numerical results) and to cover 3/4 of the cross-section (differently from experimental results but accordingly to the limit analysis method).

Using geometrical characteristics of the specimen in Eqns (1) gives

$$\tau_u / \sigma_u = 0.89; \quad (2)$$

ratio (2) allows to identify $\bar{\sigma}$ and $\bar{\tau}$ in the domain $\sigma - \tau$, shown in Fig. 14, corresponding to the same domain $\sigma_v - \sigma_o$ previously presented; the ultimate lateral force is $F_u = 12.2 \text{ t}$, whereas the normal force is $\Delta N = 6.9 \text{ t}$, in good agreement with both experimental and numerical results previously given.

5. REFERENCES

- (1) Croci G., Cerone M., "The onset of arching effect in masonry walls", Geodynamics Meeting of the National Research Council, Report no. 263, Rome, 1979.
- (2) Andreadis U., Ceradini G. D'Asdia P., "A simple model for the dynamic analysis of deteriorating structures", Proc. of the 7-th Int. Conf. on Structural Mechanics in Reactor Technology, Chicago, August 22-26, 1983, Vol. L., pp. 591-598.
- (3) Benedetti D., Casella M.L., "Shear strength of masonry piers", Proc. of the 7-th W.C.E.E., Part. III, p. 167, Istanbul, Sep. 1980.

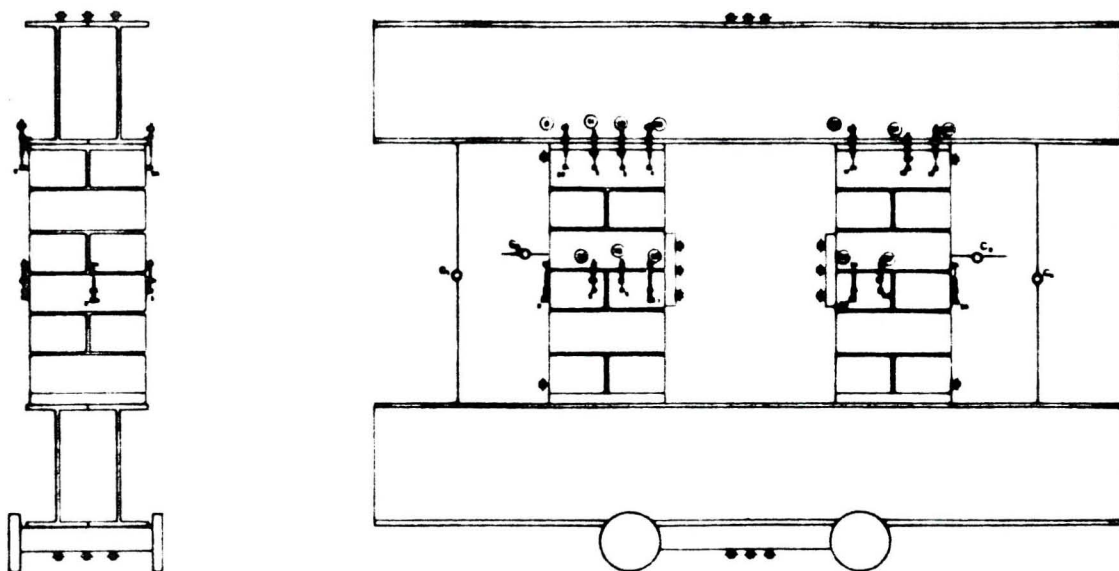


FIG. 1 - Test set

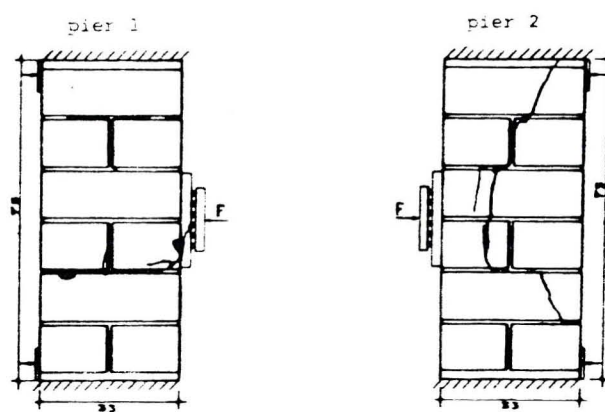


FIG. 2 - Cracking distribution at collapse

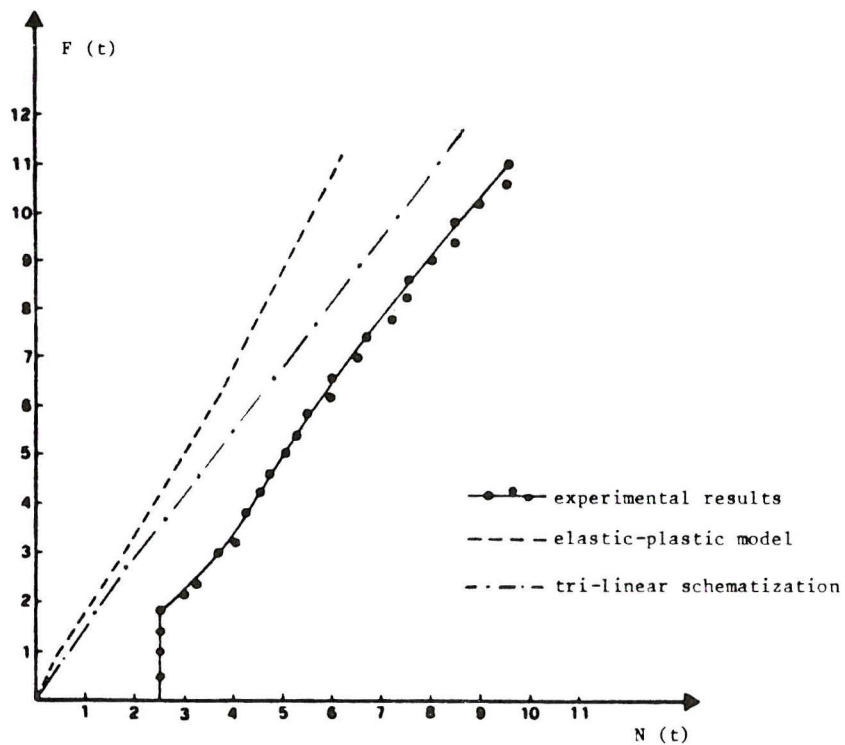


FIG. 3 - Horizontal load - axial force: comparison between experimental and numerical results.

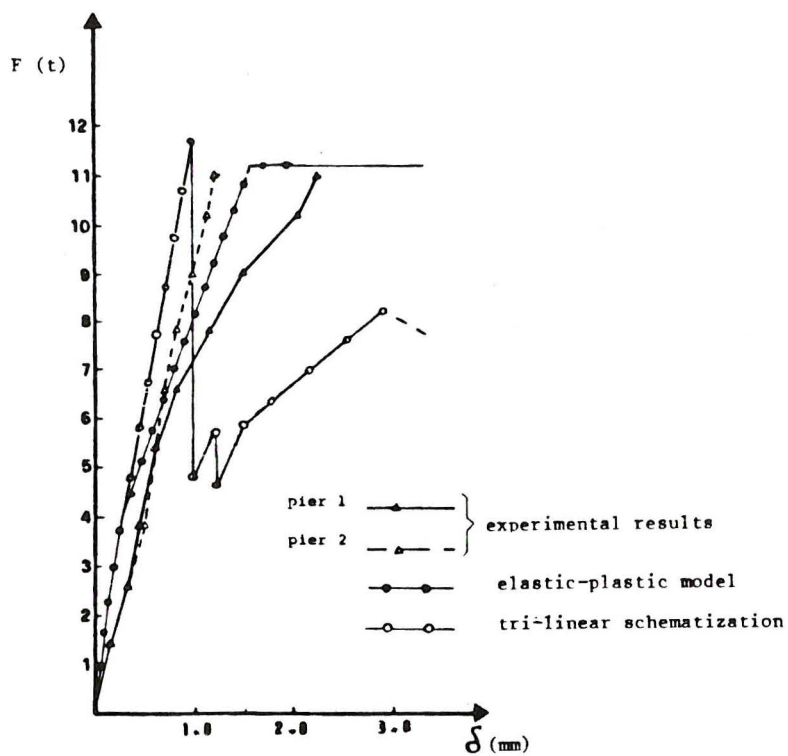


FIG. 4 - Horizontal load - middle span displacement: comparison between experimental and numerical results.

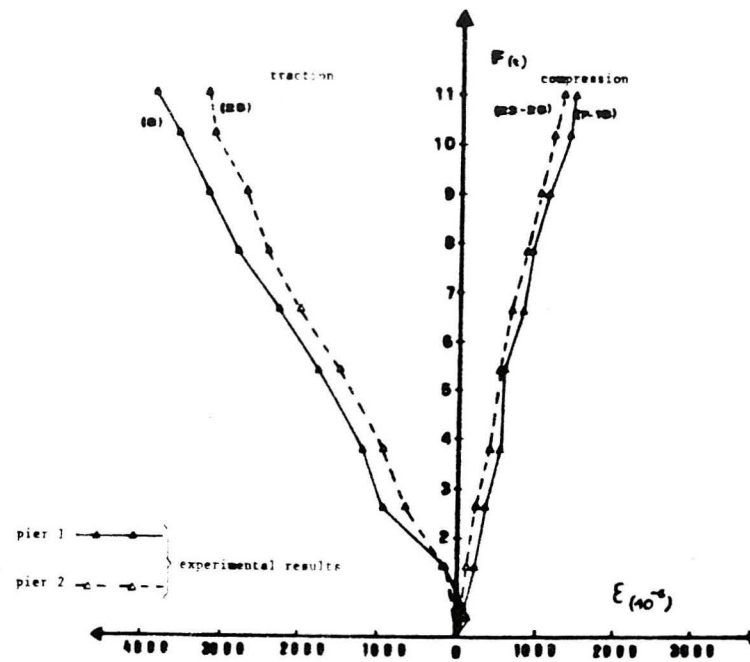


FIG. 5 - Top and bottom cross section strains versus horizontal load

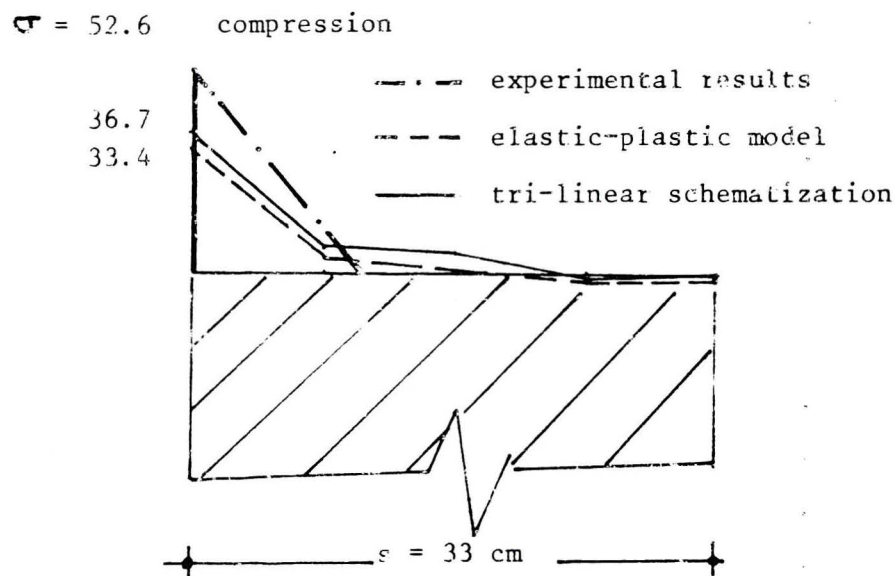


FIG. 6 - Stress distribution of middle span cross section: comparison between experimental and numerical results.

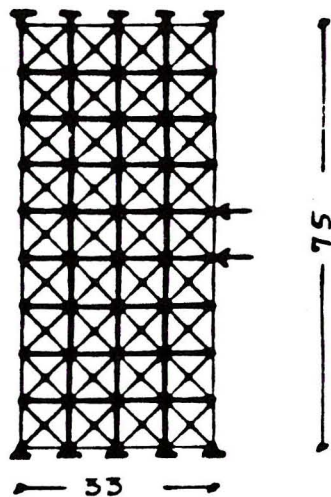


FIG. 7 - Finite element discretization.

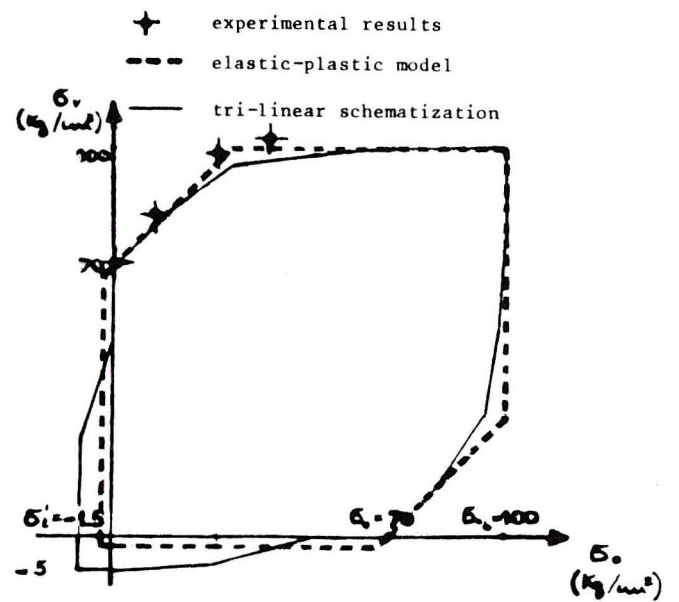


FIG. 8 - Material failure domains

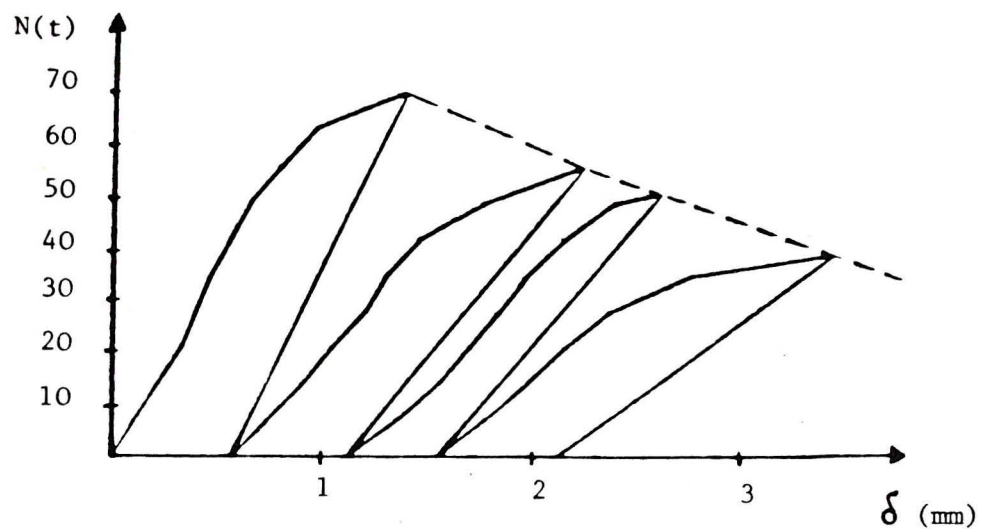


FIG. 9 - Experimental results: cyclic load.

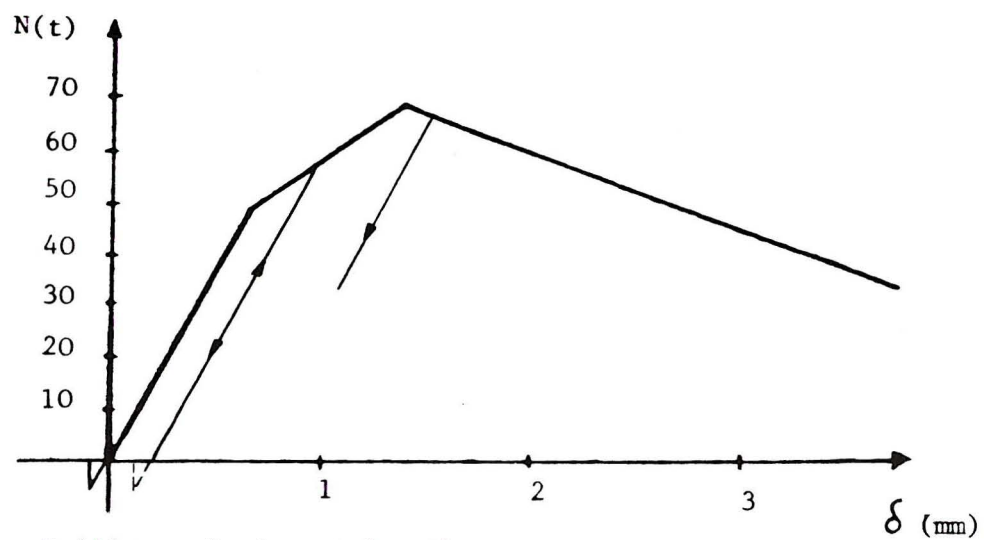


FIG. 10 - Tri-linear fundamental path.

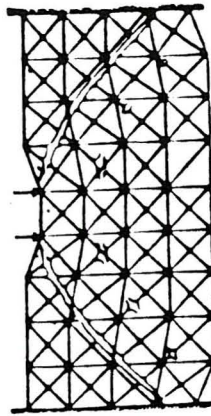


FIG. 11 - Displacement field and cracking pattern at collapse by numerical modelling.

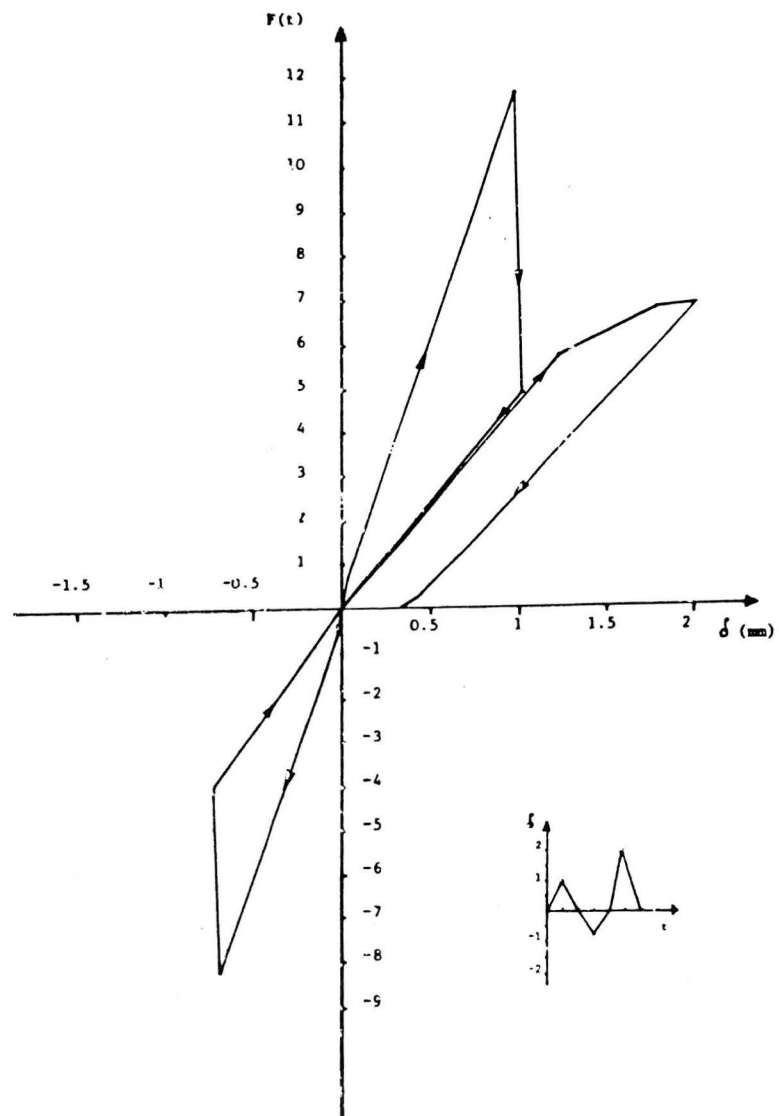


FIG. 12 - Cyclic diagrams horizontal load-middle span displacement

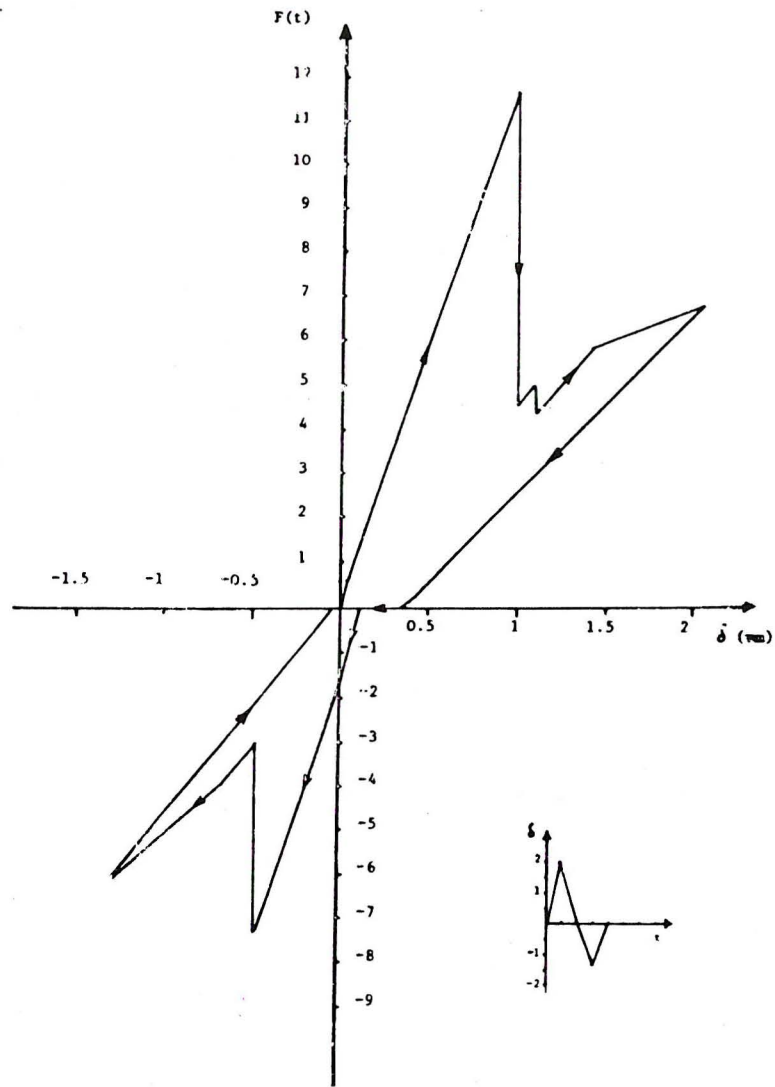


FIG. 13 - Cyclic diagrams horizontal load-midspan displacement

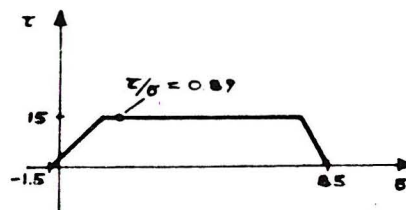


FIG. 14 - The representation collapse points in the σ - τ failure dominion